J Mater Sci (2011) 46:5260–5266
DOI 10.1007/s10853-011-5464-1

Method for effective immobilization of Ag nanoparticles/graphene oxide composites on single-stranded DNA modified gold electrode for enzymeless H_2O_2 detection

Wenbo Lu · Guohui Chang · Yonglan Luo · Fang Liao · Xuping Sun

Received: 8 January 2011 / Accepted: 10 March 2011 / Published online: 9 April 2011

Abstract In this paper, we report a new method for effective immobilization of Ag nanoparticles (AgNPs) decorated graphene oxide (AgNP/GO) composites onto thiolated single-stranded DNA decorated Au electrode (AuE) surface. The novel immobilization method is based on the coordination interactions and π–π stacking interactions between DNA bases and AgNP/GO composites. The morphologies of the AgNP/GO nanocomposites are characterized by transmission electron microscopy (TEM) and scanning electron microscopy (SEM). It is found that the AgNP/GO-decorated AuE exhibits remarkable catalytic performance for H_2O_2 reduction. This H_2O_2 sensor has a fast amperometric response time of less than 5 s. The linear range is estimated to be from 0.1 mM to 20 mM ($r = 0.998$) and the detection limit is estimated to be 1.9 μM at a signal-to-noise ratio of 3, respectively.

Introduction

In recent years, graphene oxide (GO) is emerging materials capable of delivering attractive electronic, catalytic, mechanical, optical, and magnetic properties [1–18], which can be prepared in bulk quantities by oxidative exfoliation of graphite [19, 20]. Chemical modifications of GO thus become necessary to improve its stability and introduce special functionalities [5–8]. It is extraordinary that the attachments of metal nanoparticles on graphene have offered prodigious opportunities toward emerging functions and largely expanded application areas of GO [9–18]. Particularly, Ag nanoparticles (AgNPs) decorated GO (AgNP/GO) composites have attracted immense attention. Up to now, AgNP/GO composites have been prepared by a large amount of methods, including through Ag mirror reaction [21], solution-based single-step method [22], electrostatic force directed assembly [23], and so on. These composites as prepared are a promising candidate for fundamental research as well as for potential device application such as the electrochemical sensors and biosensors [24–26]. However, the effective immobilization of AgNP/GO composites on substrate should be the first step toward such application. Up to now, only very limited immobilization methods, including layer-by-layer adsorption [27–31], self-assembly [32–36], and electrochemical deposition [37–39], have been successfully developed. Accordingly, the development of new method for rapid, effective immobilization of AgNP/GO composites on electrode is highly desired.

On the other hand, considerable attention has been paid to the detection of H_2O_2 because it is of importance in the fields of chemistry, biology, clinical control, and environmental protection [40–43]. Up to now, a variety of detection techniques have been developed, such as spectrometry [44], titrimetry [45], chemiluminescence [46], electrochemistry [47], and so on. Among them, electrochemical technique has been proven to be an inexpensive and effective way, due to its intrinsic simplicity and high sensitivity and selectivity [48, 49]. Early H_2O_2 sensors involved the use of the intrinsic selectivity and sensitivity of enzymes reactions where nanostructures are also employed to immobilize the enzymes on an electrode for maintaining the enzymatic biologic activity and electrically connecting the enzymes with the electrode surface and, at

W. Lu · G. Chang · Y. Luo · F. Liao · X. Sun (✉)
Chemical Synthesis and Pollution Control Key Laboratory of Sichuan Province, School of Chemistry and Chemical Industry, China West Normal University, Nanchong 637002, Sichuan, China
e-mail: sun.xuping@hotmail.com

the same time, to reduce the possibility of protein denaturing [50–53]. Unfortunately, the enzyme from natural sources is relatively expensive and lacks sufficient stability on the electrode surface. It has been shown that AgNPs can also exhibit good catalytic activity toward H_2O_2 reduction [32, 38, 54–56].

In this paper, by combining Au–S interactions between gold and thiol groups [57–62], coordination interactions between the nitrogen atoms of DNA bases and AgNPs [63], as well as π–π stacking interactions between DNA bases and GO [64], we develop a new method to immobilize AgNP/GO composites on Au electrode (AuE) very effectively using thiolated single-stranded DNA (thiol-ssDNA) as a linker. Scheme 1 shows a schematic to illustrate the assembly process of AgNP/GO composites on AuE by the following two steps: first, the bare AuE adsorbs thiol-ssDNA via formation of Au–S bond between Au electrode and thiol group [64]; second, AgNP/GO composites are adsorbed on thiol-ssDNA-modified AuE (ssDNA/AuE) via coordination interactions and π–π stacking interactions. It is demonstrated that the AgNP/GO-decorated AuE exhibits remarkable catalytic performance for H_2O_2 reduction due to the loading the AgNP/GO onto the AuE surface. As a result, the effective catalytic area can be tuned by the immobilization time of thiol-ssDNA and adsorption time of AgNP/GO. This H_2O_2 sensor has a fast amperometric response time of less than 5 s and its linear range and detection limit are estimated to be from 0.1 mM to 20 mM ($r = 0.998$) and 1.9 μM at a signal-to-noise ratio of 3, respectively.

Experimental details

Materials

$AgNO_3$, NaH_2PO_4, Na_2HPO_4, $KMnO_4$, graphite, ammonium hydroxide ($NH_3{\cdot}H_2O$) (28 wt% in water), H_2SO_4, sodium citrate, ethanol, KCl, $K_3[Fe(CN)_6]$, $K_4[Fe(CN)_6]$, and H_2O_2 (30%) were purchased from Aladin Ltd. (Shanghai, china). 5′-(SH)-$(CH_2)_6$-AgTCAgTgTggAAAA TCTCTAgC-3′ was purchased from Shanghai Sangon Biotechnology Co. Ltd. (Shanghai, China). Sodium citrate and sodium borohydride were purchased from Beijing Chem. Corp. All chemicals were used as received without further purification. The water used throughout all experiments was purified through a Millipore system. Phosphate buffer saline (PBS) was prepared by mixing stock solutions of NaH_2PO_4 and Na_2HPO_4 and fresh solution of H_2O_2 was prepared daily.

Preparation of GO

Graphene oxide (GO) was prepared from natural graphite powder through a modified Hummers method [19]. In a typical synthesis, 1 g of graphite was added into 23 mL of 98% H_2SO_4, followed by stirring at room temperature over a 24 h period. After that, 100 mg of $NaNO_3$ was introduced into the mixture and stirred for 30 min. Subsequently, the mixture was kept below 5 °C by ice bath, and 3 g of $KMnO_4$ was slowly added into the mixture. After being heated to 35–40 °C, the mixture was stirred for another 30 min. After that, 46 mL of water was added into above mixture during a period of 25 min. Finally, 140 mL of water and 10 mL of 30% H_2O_2 were added into the mixture to stop the reaction. After the unexploited graphite in the resulting mixture was removed by centrifugation, as-synthesized GO was dispersed into individual sheets in distilled water at a concentration of 0.5 mg/mL with the aid of ultrasound for further use.

Preparation of AgNP/GO composites

AgNP/GO composites were prepared by the reduction of silver ions in the GO dispersion solution, according to established method [65]. In brief, 0.2 mL of 0.01 M $AgNO_3$ aqueous solution was introduced into 5 mL of 0.25 mg/mL GO dispersion solution and then magnetically stirring for 30 min. Subsequently, 10 mL of 0.8 mg/mL alkaline solution of sodium borohydride (pH 9.5) was added to the GO dispersion solution under stirring vigorously at room temperature for 2 h. A clear brown dispersion of AgNP/GO was formed, and the resulting dispersion was stored at 4 °C for characterization and further use.

Apparatus

UV–vis spectra were collected on a UV5800 modal spectrophotometer. Transmission electron microscopy (TEM) measurements were made on a HITACHI H-8100 EM (Hitachi, Tokyo, Japan) with an accelerating applied potential of 200 kV. The sample for TEM characterization was prepared by place a drop of the dispersion on carbon-coated copper grid and dried at room temperature.

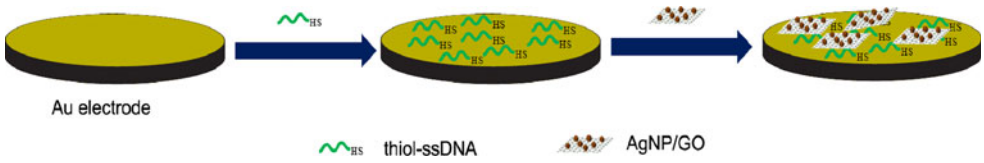

Scheme 1 A schematic illustrating the assembly process of AgNP/GO on AuE

Electrochemical measurements are performed with a CHI 660D electrochemical analyzer (CH Instruments, Inc., Shanghai). A conventional three-electrode cell is used, including a Au electrode (AuE, 2 mm in diameter) as the working electrode, a Ag/AgCl (3 M KCl) electrode as the reference electrode, and platinum foil as the counter electrode. All potentials given in this work are referred to the Ag/AgCl electrode. All the experiments are carried out at ambient temperature.

Electrode modification

The surface of AuE was polished with 1.0 and 0.3 μm α-alumina powders in sequence, rinsed thoroughly with twice distilled water, and placed in a water-filled ultrasonic bath over a 1-min period. Then the electrode surface was cleaned by electrochemical sweeping in 0.5 M H_2SO_4 from 0 to 1.8 V until a reproducible cyclic voltammogram was obtained. Then it was rinsed with water, and ultrasonicated for 1 min in ethanol and water, respectively. In the typical experiment, 2 μL of 20 μM thiol-ssDNA PBS solution (pH 7.4) was dropped on the surface of AuE, followed by storage at 4 °C for 30 min. After removing the excess thiol-ssDNA by washing with distilled water, 2 μL of AgNP/GO composites were dropped onto the surface of AuE, followed by storage at 4 °C for 30 min. After the modified electrode was rinsed with twice distilled water, the AgNP/GO composites decorated AuE was obtained.

Results and discussion

Figure 1 shows the UV–vis absorption spectra of GO and AgNP/GO dispersion. It is obviously seen that the GO dispersion exhibits two characteristic peaks, a maximum at 230 nm, which corresponds to $\pi \rightarrow \pi^*$ transitions of aromatic C–C bonds, and a shoulder at 300 nm, which is attributed to $n \rightarrow \pi^*$ transitions of C=O bonds (Fig. 1 curve a) [65, 66]. A peak at 261 nm is observed in the AgNP/GO dispersion, as shown in Fig. 1 (curve b). It can be attributed to the peak at 230 nm in the GO dispersion red shifted, indicating that the GO in the AgNP/GO dispersion is partially reduced after adding the sodium borohydride and silver ions [65]. A peak at 405 nm is also observed in Fig. 1 (curve b), which is attributed to the AgNPs as formed [65]. All these observations indicate the AgNP/GO composites are formed.

Figure 2a shows typical SEM image of the AgNP/GO composites formed by the GO incubation with a $AgNO_3$ and sodium borohydride aqueous solution over a 2-h period. It is clearly seen that a large amount of AgNPs (white dots) adsorbed on these GO nanosheets. Such observation is also evidenced by the high magnification image, as

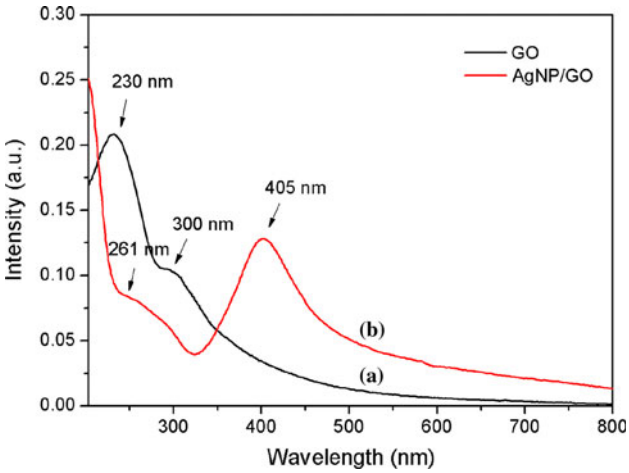

Fig. 1 UV–vis absorption spectra of (*a*) GO and (*b*) AgNP/GO composites

shown in Fig. 2b. It is clearly seen that these AgNPs on the GO sheets are spherical in shape and range from 50 to 60 nm, but fail to observe the AgNPs less than 50 nm in size by the SEM analysis. The chemical composition of the AgNP/GO composites was also determined by the corresponding energy-dispersive spectrum (EDS) (Fig. 2c). Two peaks of C and O elements are observed, indicating that they are products formed from GO, and three peaks of Ag element are also observed, indicating that the AgNPs are successfully adsorbed on the GO nanosheets. Other peaks are originated from the glass substrate used. All the above observations indicate that the AgNP/GO composites are constructed.

To get further information on the products thus obtained, we examined the dispersion by TEM analysis. Figure 3a shows the low magnification image of the AgNP/GO composites, indicating the GO nanosheet with the lateral dimensions is about 1.5 μm. Please note that a large number of small black dots are observed on the GO nanosheets. A high magnification image further reveals that these AgNPs are ranging from 10 to 50 nm in size and spherical in shape, as shown in Fig. 2b. All these observations indicate that AgNP/GO composites are formed. Based on the TEM analysis, it is clearly seen that the main components in such dispersion contain GO coated by AgNPs. The GO nanosheets are provided with hydroxyl and epoxy functional groups located at the nanosheets edges [67]. The functional groups have been used as anchors for adsorption of polar materials and inorganic nanoparticles [68, 69]. As a result, the positive Ag^+ ion can easily adsorb onto these negative GO sheets through electrostatic attraction [70]. The reduction of these ions by sodium borohydride allows these AgNPs to attach onto the GO nanosheets. Most of the AgNPs deposited onto the surface of the GO nanosheets.

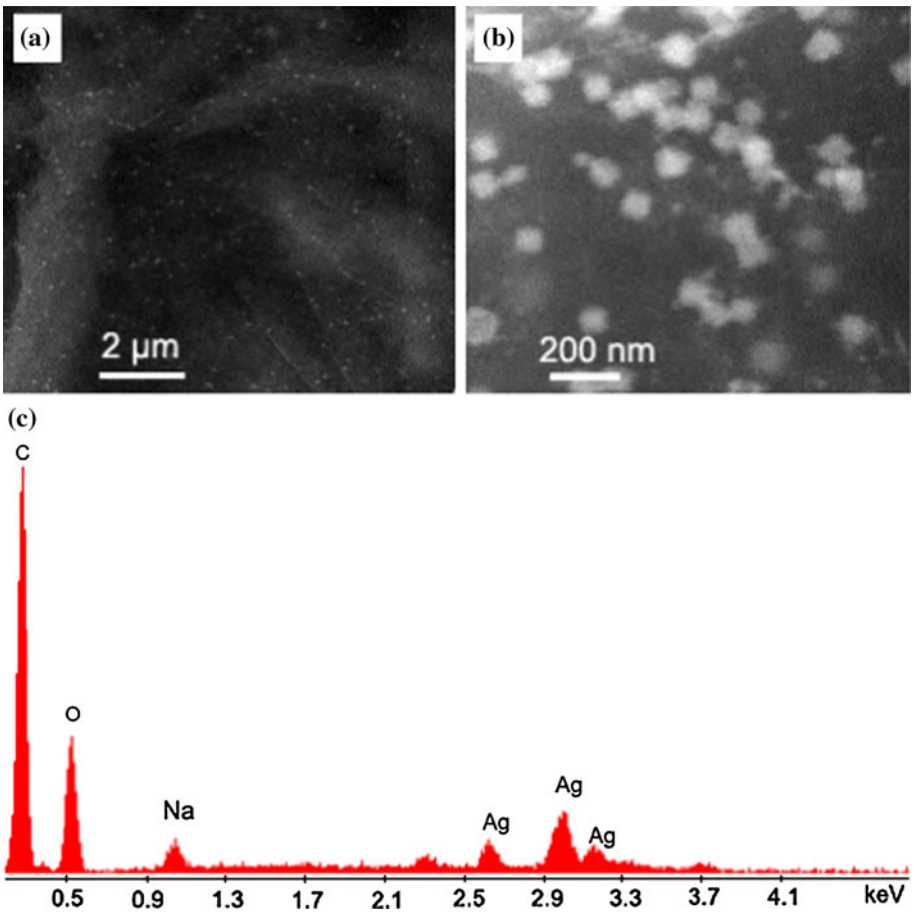

Fig. 2 **a** Low and **b** high magnification SEM images of the AgNP/GO composites. **c** The corresponding EDS of the AgNP/GO composites

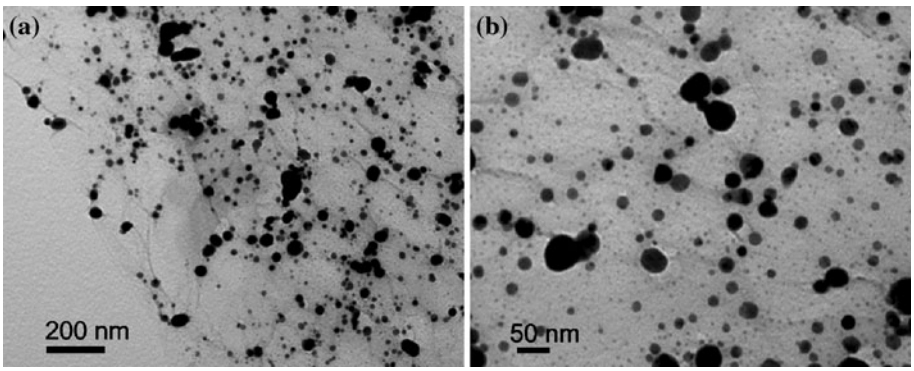

Fig. 3 **a** Low and **b** high magnification TEM images of the AgNP/GO composites

Figure 4 shows the cyclic voltammetric responses of the bare AuE, AuE decorated with thiol-ssDNA (ssDNA/AuE), and AuE decorated with thiol-ssDNA and AgNP/GO (AgNP/GO/ssDNA/AuE) in 0.01 M KCl aqueous solution containing 5 mM $[Fe(CN)_6]^{4-}$ and 5 mM $[Fe(CN)_6]^{3-}$ at a scan rate of 0.05 V/s. The bare AuE exhibits a pair of well-defined reduction/oxidation peaks, as shown in Fig. 4 (line a). After the immobilization of thiol-ssDNA for 30 min on AuE surface, a decrease in anodic peak current and cathodic peak is observed (Fig. 4 line c), which can be attributed to that thiol-ssDNA formed a film with low coverage and the electrostatic repulsion interactions between its negatively charged backbone and $[Fe(CN)_6]^{4-/3-}$ blocked the diffusion of ferricyanide toward the electrode surface to some extent [71]. During immobilization of AgNP/GO onto thiol-ssDNA decorated AuE (Fig. 4 line b), it is clearly observed a decrease in anodic peak current and cathodic peak compared with the bare AuE (Fig. 4 line a) and an increase compared with AuE decorated with thiol-ssDNA (Fig. 4 line c). It is apparently seen that immobilization of AgNP/GO onto the thiol-ssDNA decorated AuE has markedly promoted the electron transfer of the system owing to formation of a continuous film of AgNP/GO via thiol-ssDNA on the AuE. However, it is interestingly found

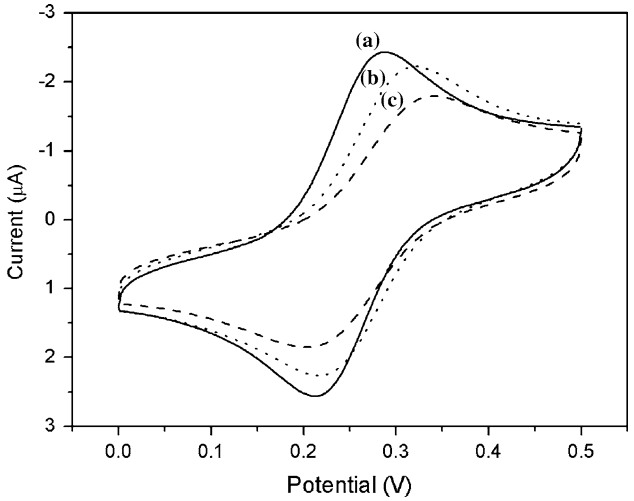

Fig. 4 Cyclic voltammograms (CVs) of (*a*) bare AuE and (*b*) the ssDNA/AuE with immobilization time 30 min after further attachment of AgNP/GO (*c*) ssDNA/AuE with immobilization time of 30 min in 0.01 M KCl aqueous solution containing 5 mM $[Fe(CN)_6]^{4-}$ and 5 mM $[Fe(CN)_6]^{3-}$ (scan rate: 0.05 V/s)

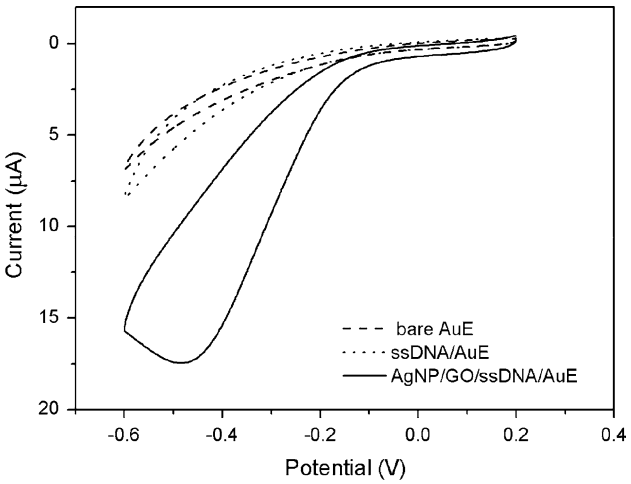

Fig. 5 CVs of a bare AuE, ssDNA/AuE, and the AgNP/GO/ssDNA/AuE in 0.2 M N_2-saturated PBS at pH 7.4 in the presence of 1.0 mM H_2O_2 (scan rate: 0.05 V/s)

that the AgNP/GO has highly π electron as a result of repulsing the negatively charged $[Fe(CN)_6]^{3-}$ and $[Fe(CN)_6]^{4-}$, interfering with the diffusion of ferricyanide toward to the AuE surface [72].

We designed an enzymeless H_2O_2 sensor by immobilizing AgNP/GO on AuE using thiol-ssDNA as a linker. Figure 5 shows the electrocatalytic responses of a bare AuE, ssDNA/AuE, and the AgNP/GO/ssDNA/AuE toward the reduction of H_2O_2 in N_2-saturated 0.2 M PBS at pH 6.5 in the presence of 1.0 mM H_2O_2. We also performed one control experiment by studying the cyclic voltammograms (CVs) behavior of AgNP/GO/ssDNA/AuE in the absence of H_2O_2. In the presence of 1 mM H_2O_2, the AgNP/GO/ssDNA/AuE exhibits a notable current peak centered at −0.48 V versus Ag/AgCl; however, it exhibits no electrochemical response in the absence of H_2O_2. These observations indicate that the observed current peak originates from H_2O_2 reduction. Nevertheless, the responses of both the bare AuE and ssDNA/AuE toward the reduction of H_2O_2 are quite weak and even can be neglected. All the above observations indicate that the AgNP/GO adsorbed on the thiol-ssDNA decorated AuE surface exhibits a notable catalytic performance for H_2O_2 reduction, and the large catalytic current obtained could be attributed to the large numbers of AgNPs/GO contained therein. Compared to glassy carbon electrode modified by simple electroreduction of Ag^+ [54], the AgNP/GO/ssDNA/AuE exhibits a 12.5% enhancement of peak current and a 30 mV positive shift of the peak potential. In addition, the relative standard deviation (RSD) of the amperometric response to 1 mM H_2O_2 was 3.9% for five successive measurements, indicating the good reproducibility of the AgNP/GO/ssDNA/AuE.

To examine the influence of immobilization time of thiol-ssDNA on the electrocatalytic reduction of H_2O_2, the Au electrodes were prepared with various immobilization time of thiol-ssDNA ranging from 5 to 60 min. Figure 6a shows the relation between the peak currents obtained and immobilization time of thiol-ssDNA. It is clearly seen that the reduction peaks increased linearly with increasing the immobilization of thiol-ssDNA time ranging from 5 to 40 min, however, the reduction peak decreased with increasing the immobilization time of thiol-ssDNA ringing from 40 to 60 min. It is found that the optimal condition of the immobilization of thiol-ssDNA time is 40 min. Meanwhile, we also examine the influence of the adsorption time of AgNP/GO on the electrocatalytic reduction of H_2O_2. Figure 6b shows the relation between the adsorption time and the peak currents. It is found that the reduction peak currents toward H_2O_2 increase sharply with increasing the adsorption time of AgNP/GO ranging from 5 to 40 min. However, the peak currents increase sluggishly and tend to a stable value with further increasing of the adsorption time from 40 to 50 min. All the above observations indicate that increased adsorption time leads to increased adsorption of AgNPs on the ssDNA/AuE and the saturation is reached over a 40-min period.

Figure 7 shows typical current–time plot of the AgNP/GO/ssDNA/AuE in N_2-saturated 0.2 M PBS buffer (pH 7.4) on consecutive step change of H_2O_2 concentrations under the above optimized conditions. When an aliquot of H_2O_2 was dropped into the stirring PBS solution, the reduction current rose steeply to reach a stable value. The sensor could accomplish 96% of the steady-state current within 5 s, indicating a fast amperometric response

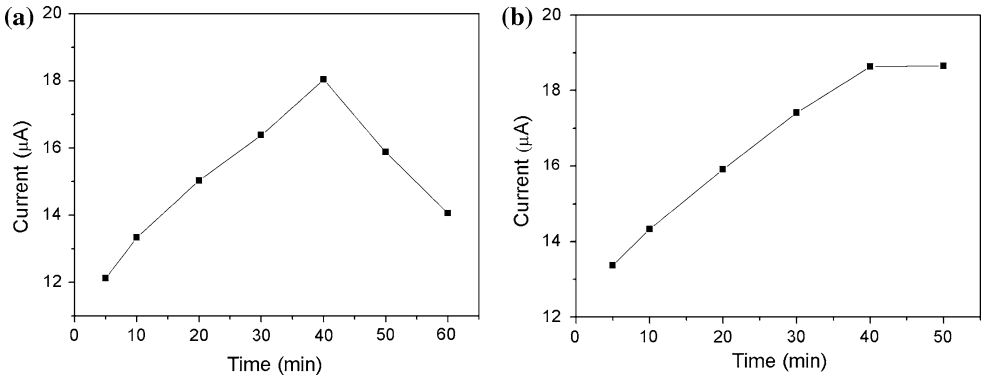

Fig. 6 The influence of immobilization time of thiol-ssDNA (**a**) and the adsorption time of AgNPs (**b**) on the cyclic voltammetric responses of resulting AgNP/GO/ssDNA/AuE in 0.2 M PBS at pH 7.4 in the presence of 1.0 mM H_2O_2 (scan rate: 0.05 V/s). When one parameter changed the other parameter was at their optimal values

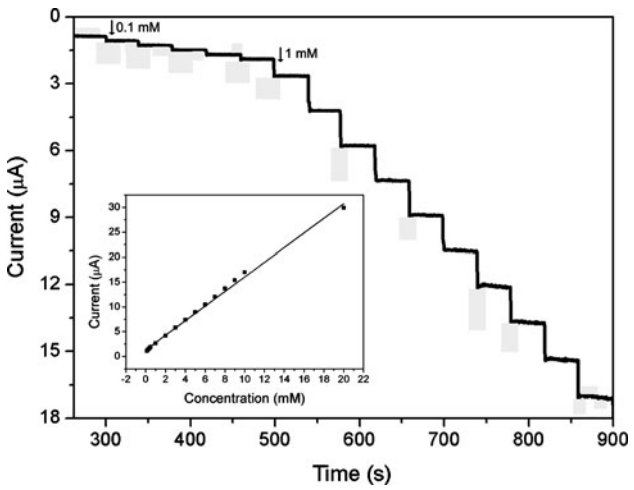

Fig. 7 Typical steady-state response of the AgNP/GO/ssDNA/AuE to successive injection of H_2O_2 into the stirred N_2-saturated 0.2 M PBS at pH 7.4 (Applied potential: −0.30 V). *Inset*: the fitting of the experimental data by the regression line

behavior. It is apparently seen that the steps showed in Fig. 7 are more horizontal in the region of lower concentration of H_2O_2 and the noises become higher with increased concentration of H_2O_2. The inset in Fig. 7 shows the calibration curve of the sensor. The linear detection range is estimated to be from 0.1 mM to 20 mM ($r = 0.998$), and the detection limit is estimated to be 1.9 μM at a signal-to-noise ratio of 3. Compared to our previous work, the detection limit of the H_2O_2 sensor designed herein is lower than AgNP-decorated graphene nanosheets [32], AgNP-decorated nanofibers [56], and the PQ11-AgNPs [55].

Conclusions

In conclusion, by combining Au–S interactions between gold and thiol group and coordination interactions and π-conjugated effect between the DNA bases and AgNP/GO, we demonstrate a new method to immobilize AgNP/GO on AuE very effectively using thiol-ssDNA as a linker. Most importantly, it is found that the resultant modified electrode exhibits remarkable catalytic ability toward H_2O_2 reduction. Our present stduy provides us a new methodology to immobilize AgNP/GO on electrode for applications.

References

1. Novoselov KS, Geim AK, Morozov SV, Jiang D, Zhang Y, Dubonos SV, Grigorieva IV, Firsov AA (2004) Science 306:666
2. Robinson JT, Zalalutdinov M, Baldwin JW, Snow ES, Wei ZQ, Sheehan P, Houston BH (2008) Nano Lett 8:3441
3. Stankovich S, Dikin DA, Dommett GHB, Kohlhaas KM, Zimney EJ, Stach EA, Piner RD, Nguyen ST, Ruoff RS (2006) Nature 442:282
4. Zhang Y, Small JP, Amori MES, Kim P (2005) Phys Rev Lett 94:176803
5. Liu Z, Robinson JT, Sun XM, Dai HJ (2008) J Am Chem Soc 130:10876
6. Lomeda JR, Doyle CD, Kosynkin DV, Hwang WF, Tour JM (2008) J Am Chem Soc 130:16201
7. Zhang M, Yin BC, Tan WH, Ye BC (2011) Biosens Bioelectron 26:3260
8. Li XL, Wang XR, Zhang L, Lee SW, Dai HJ (2008) Science 319:1229
9. Scheuermann GM, Rumi LG, Steurer P, Bannwarth W, Mulhaupt R (2009) J Am Chem Soc 131:8262
10. Jasuja K, Berry V (2009) ACS Nano 3:2358
11. Kong BSZ, Geng JX, Jung HT (2009) Chem Commun 2174
12. Li YM, Tang LH, Li JH (2009) Electrochem Commun 11:846
13. Liu JB, Li YL, Li YM, Li JH, Deng ZX (2010) J Mater Chem 20:900
14. Paek SM, Yoo EJ, Honma I (2009) Nano Lett 9:72
15. Seger B, Kamat PV (2009) J Phys Chem 113:7990
16. Hong WJ, Bai H, Xu YX, Yao ZY, Gu ZZ, Shi GQ (2010) J Phys Chem C 114:1822
17. Jang BZ, Zhamu A (2008) J Mater Sci 43:5092. doi:10.1007/s10853-008-2755-2
18. Liu J, Fu S, Yuan B, Li Y, Deng Z (2010) J Am Chem Soc 132:7279
19. Hummers WS, Offeman RE (1958) J Am Chem Soc 80:1339
20. Chung DDL (2002) J Mater Sci 37:1475. doi:10.1023/A:1014915307738
21. Xu C, Wang X (2009) Small 19:121117
22. Pasricha R, Gupta S, Srivastava AK (2009) Small 5:253
23. Lu G, Mao S, Park S, Ruoff RS, Chen J (2009) Nano Res 2:192

24. Jin E, Lu X, Cui L, Chao D, Wang C (2010) Electrochim Acta 55:7230
25. Wang Y, Shao Y, Matson D, Li J, Lin Y (2010) ACS Nano 4:1790
26. Kang X, Wang J, Wu H, Aksay IA, Liu J, Lin Y (2009) Biosens Bioelectron 25:901
27. Cassagneau T, Fendler JH (1999) J Phys Chem B 103:1789
28. Ji Q, Honma I, Paek SM, Akada M, Hill AJ, Vinu A, Ariga K (2010) Angew Chem Int Ed 49:9737
29. Zeng GH, Xing YB, Gao J, Wang ZQ, Zhang X (2010) Langmuir 26:15022
30. Zhu CZ, Guo SJ, Zhai YM, Dong SJ (2010) Langmuir 26:7614
31. Dai JH, Bruening ML (2002) Nano Lett 2:497
32. Liu S, Tian JQ, Wang L, Li HL, Zhang YW, Sun XP (2010) Macromolecules 43:10078
33. Yang SL, Xu BF, Zhang JQ, Huang XD, Ye JS, Yu CZ (2010) J Phys Chem C 114:4389
34. Fang YX, Guo SJ, Zhu CZ, Zhai YM, Wang EK (2010) Langmuir 26:11277
35. Welch CM, Banks CE, Simm AO, Compton RG (2005) Anal Bioanal Chem 382:12
36. Zhou XZ, Huang X, Qi XY, Wu SX, Xue C, Boey FYC, Yan QY, Chen P, Zhang H (2009) J Phys Chem C 113:10842
37. Zhou YG, Chen JJ, Wang FB, Sheng ZH, Xia XH (2010) Chem Commun 46:5951
38. Song YH, Cui K, Wang L, Chen SH (2009) Nanotechnology 20:105501
39. Wu S, Zhao HT, Shi CG, Zhao JW, Ju HX (2006) Electrochem Commun 8:1197
40. Luo X, Xu J, Zhao W, Chen H (2004) Biosens Bioelectron 19:1295
41. Cipriano TC, Takahashi PM, Lima D, Oliveira VX Jr, Souza JA, Martinho H, Alves WA (2010) J Mater Sci 45:5101. doi: 10.1007/s10853-010-4478-4
42. Lu X, Zhou J, Lu W, Liu Q, Li J (2008) Biosens Bioelectron 23:1236
43. Shu X, Chen Y, Yuan H, Gao S, Xiao D (2007) Anal Chem 79:3695
44. Matsubara C, Kawamoto N, Takamura K (1992) Analyst 117:1781
45. Hurdis CH, Romeyn H (1954) Anal Chem 26:320
46. Nakashima K, Maki K, Kawaguohi S, Akiyama S, Tsukamoto Y, Kazuhiro I (1991) Anal Sci 7:709
47. Chen SH, Yuan R, Chai YQ, Zhang LY, Wang N, Li XL (2007) Biosens Bioelectron 22:1268
48. Jia JB, Wang BQ, Wu AG, Cheng GJ, Li Z, Dong SJ (2002) Anal Chem 74:2217
49. Luo XL, Xu J, Zhang Q, Yang GJ, Chen HY (2005) Biosens Bioelectron 21:190
50. Song Y, Wang L, Ren C, Zhu G, Li Z (2006) Sens Actuators B 114:1001
51. Guo C, Song Y, Wei H, Li P, Wang L, Sun L, Sun Y, Li Z (2007) Anal Bioanal Chem 389:527
52. Willner I, Katz E (2000) Angew Chem Int Ed 39:1180
53. Xiao Y, Patolsky F, Katz E, Hainfeld J, Willner I (2003) Science 299:1877
54. Lu WB, Liao F, Luo YL, Chang GH, Sun XP (2011) Electrochim Acta 56:2295
55. Tian JQ, Liu S, Sun XP (2010) Langmuir 26:15112
56. Tian JQ, Li HL, Lu WB, Luo YL, Wang L, Sun XP (2011) Analyst (accepted for publication)
57. Kelley SO, Barton JK, Jackson NM, Mcpherson LD, Potter AB, Spain EM, Allen MJ, Hill MG (1998) Langmuir 14:6781
58. Herne TM, Tarlov MJ (1997) J Am Chem Soc 119:8916
59. Yang M, Yau HCM, Chan HL (1998) Langmuir 14:6121
60. Okahata Y, Matsunobu Y, Kunihara I, Masayuki M, Murakami A, Makino K (1992) J Am Chem Soc 114:8299
61. Tarlov MJ, Newman JG (1992) Langmuir 8:1398
62. Georgiadis R, Peterlinz KP, Peterson AW (2000) J Am Chem Soc 122:3166
63. Wang Y, Yang F, Yang XR (2010) ACS Appl Mater Int 2:339
64. Lu C, Yang H, Zhu C, Chen X, Chen G (2009) Angew Chem Int Ed 48:4785
65. Li J, Liu C (2010) Eur J Inorg Chem 1244
66. Paredes JI, Villar-Rodil S, Martinez-Alonso A, Tascon JMD (2008) Langmuir 24:10560
67. Szabo T, Berkesi O, Forgo P, Josepovits K, Sanakis Y, Petridis D, Dekany I (2006) Chem Mater 18:2740
68. Xu C, Wang X, Zhu JW, Yang XJ, Lu LD (2008) J Mater Chem 18:5625
69. Herrera-Alonso M, Abdala AA, McAllister MJ, Aksay IA, Prudhomme RK (2007) Langmuir 23:10644
70. Yang XJ, Makita YJ, Liu ZH, Ooi K (2003) Chem Mater 15:1228
71. Yau HCM, Chan HL, Sui S, Yang M (2002) Thin Solid Film 413:218
72. Zhang SX, Wang N, Niu YM, Sun CQ (2005) Sens Actuators B 109:367